



OPEN

Direct Laser Writing of Nanodiamond Films from Graphite under Ambient Conditions

SUBJECT AREAS:
APPLIED PHYSICS
MATERIALS SCIENCEReceived
5 June 2014Accepted
19 September 2014Published
20 October 2014Correspondence and
requests for materials
should be addressed to
G.J.C. (gjcheng@
purdue.edu)Qiong Nian¹, Yuefeng Wang², Yingling Yang¹, Ji Li¹, Martin Y. Zhang¹, Jiayi Shao³, Liang Tang³
& Gary J. Cheng^{1,4,5}¹School of Industrial Engineering, Purdue University, West Lafayette, IN, USA, ²School of Materials Engineering, Purdue University, West Lafayette, IN, USA, ³Department of Physics, Purdue University, West Lafayette, IN, USA, ⁴School of Mechanical Engineering, Purdue University, West Lafayette, IN, USA, ⁵Birck nanotechnology Center, Purdue University, West Lafayette, IN, USA.

Synthesis of diamond, a multi-functional material, has been a challenge due to very high activation energy for transforming graphite to diamond, and therefore, has been hindering it from being potentially exploited for novel applications. In this study, we explore a new approach, namely confined pulse laser deposition (CPLD), in which nanosecond laser ablation of graphite within a confinement layer simultaneously activates plasma and effectively confine it to create a favorable condition for nanodiamond formation from graphite. It is noteworthy that due to the local high dense confined plasma created by transparent confinement layer, nanodiamond has been formed at laser intensity as low as 3.7 GW/cm², which corresponds to pressure of 4.4 GPa, much lower than the pressure needed to transform graphite to diamond traditionally. By manipulating the laser conditions, semi-transparent carbon films with good conductivity (several kΩ/Sq) were also obtained by this method. This technique provides a new channel, from confined plasma to solid, to deposit materials that normally need high temperature and high pressure. This technique has several important advantages to allow scalable processing, such as high speed, direct writing without catalyst, selective and flexible processing, low cost without expensive pico/femtosecond laser systems, high temperature/vacuum chambers.

Diamond, a multi-functional material, is of extreme scientific interest¹⁻⁵. New promising applications, such as biosensor¹, quantum computing², fuel cell³ and next generation of computer chip⁴ have been identified. However, diamond materials are difficult to be synthesized from graphite, due to very high activation energy for graphite-diamond transition and the diamond phase is unstable in low profile conditions. Thus, the synthesis of diamond requires extreme environments⁵⁻⁷ like high temperature (>2000 K) and high pressure (>10 GPa). Various synthesis techniques have been developed to synthesize diamond materials, e.g., high temperature high pressure⁸, detonation synthesis⁹, and chemical vapor deposition (CVD)¹⁰ and laser assisted methods¹¹⁻¹³. However, these methods are usually limited to high cost and low yield due to the requirement of keeping extreme environments^{6,7,14}. Synthesis of diamond materials, especially under moderate conditions; thus remains a challenging task. Currently, one of the major goals in diamond materials research is to lower the operating temperature, increase the growth rate and reduce the fabrication cost^{5,6,14}.

Attempting to explore a novel approach to synthesize diamond materials under moderate conditions, we employed transparent solid confinements to impede the expansion of carbon vapor during ultra-fast laser ablation. The maximum thermal pressure of carbon vapor can dominantly be affected by the time scale of heating¹⁵. With ultra-fast laser ablation, graphite phase carbon is able to expand with a speed of 2.3 mm/μs. Considering an idealistic condition, the thermal shock generated by ultra-fast laser pulse (nano/picosecond) is so intense and short that the external structure has not enough time to expand. In the iso-volumetric process, the total rise of molar volume due to thermal expansion could be suppressed by an equivalent thermal pressure. The instantaneous temperature rise is able to create an enormous pressure of more than 2 up to 100 GPa, which is enough for the metastable carbon plasma plume formation and graphite-diamond phase transformation^{15,16}. In this work, a transparent solid confinements were utilized to impede the laser ablated thermal expansion, leading to a localized extreme condition close to iso-volumetric process. The impeded carbon expansion results in localized high pressure to trigger transformation of graphite to nanodiamond, with relative low laser intensity of >4.4 GW/cm² rather than Nagel criterion threshold of 50 GW/cm².



The operation is performed at room temperature and atmospheric pressure, during which, the confinement of hot vapor creates this localized extreme environment¹⁷. Such localized extreme environment helps to achieve high activation energy needed for diamond phase carbon formation. As stated by prior studies, nanodiamond has higher stability compared to graphite at particle size of a few nm^{18,19}, suggesting the potential to synthesize nanodiamond from graphite at ambient conditions.

Results

Resulting from the localized extreme environment in our study, nanodiamond particles formed in a matter of just few tens of nanoseconds under rapid heating and quenching. Semi-transparent and conductive carbon film was also obtained by manipulating the laser parameters. This laser processing technique has several advantages, including high speed, high flexibility, low cost and avoids energy loss. For example, no high vacuum equipment or protective atmosphere is required and the process is highly flexible, convenient yet very precise; since the locations and directions can be controlled. Thus, the processing conditions of lithography could easily be manipulated.

The setup of confined pulse laser deposition (CPLD), as we have termed the phenomena and representative optical images of carbon films are shown in Figure 1. When the laser intensity is below the critical value (3.7 GW/cm^2), the carbon films obtained by CPLD look semi-transparent and have metallic luster (Figure 1d), which is similar to HOPG (highly oriented pyrolytic graphite). As the laser intensity is increased beyond a critical value, the carbon films obtained by CPLD become more transparent, and the metallic luster disappears. Figure 2(a–c) shows the typical SEM images of the transparent carbon film processed at laser intensity of 5.8 GW/cm^2 . The SEM images reveal that these dense carbon particles are nanocrystals with distinguishable growth faces, which exhibit different microstructures

as compared to graphite particles. Several characterization tools were employed to analyze these carbon films. In brief, microscopy such as scanning electron microscopy (SEM), transmission electron microscopy (TEM), X-ray diffraction and spectroscopic techniques such as UV-VIS-NIR transmission spectroscopy and X-ray photoemission spectroscopy (XPS) and electronic conductivity measurements were employed. Based on these characterizations, we conclude that these carbon films are composed of nanodiamond particles and a certain amount of graphite like carbon. The laser intensity used in the present experiment was comparatively lower ($>3.7 \text{ GW/cm}^2$) than the Nagel criterion threshold which is 50 GW/cm^2 for laser having wavelength of 1064 nm . Yet, we have clear evidence of nanodiamond formation. During CPLD process, the vaporization of graphite destroys the crystalline order of graphite and greatly reduces the dynamic barrier for synthesizing diamond phase carbon. Furthermore, the ionization and condensation of explosive carbon vapor create highly active intermediate species that eventually helps in the formation of nanodiamond.

The difference in free energies between graphite and diamond is about 2.5 kJ/mol at 0 K and atmosphere pressure, which is far less than the free energy of carbon vapor ($\sim 712 \text{ kJ/mol}$)²⁰. This means the conversion of carbon vapor to diamond and to graphite would almost have the same probability under thermal equilibrium. There have been many attempts to find possible ways to condense carbon vapor. However, these efforts were usually unsuccessful²⁰. During past three decades, it has been observed that activated plasma containing energetic species enables selective formation of diamond from vapor phase^{14,21,22}. For example, Palnichenko *et al.*²² demonstrated diamond formation from carbon vapor. The diamond is generated by thermal activation of graphite using electric pulse discharge. Vincent *et al.*²³ built a bottom-up approach to synthesize the nanodiamond with nanostructured explosives. Recently, it has been

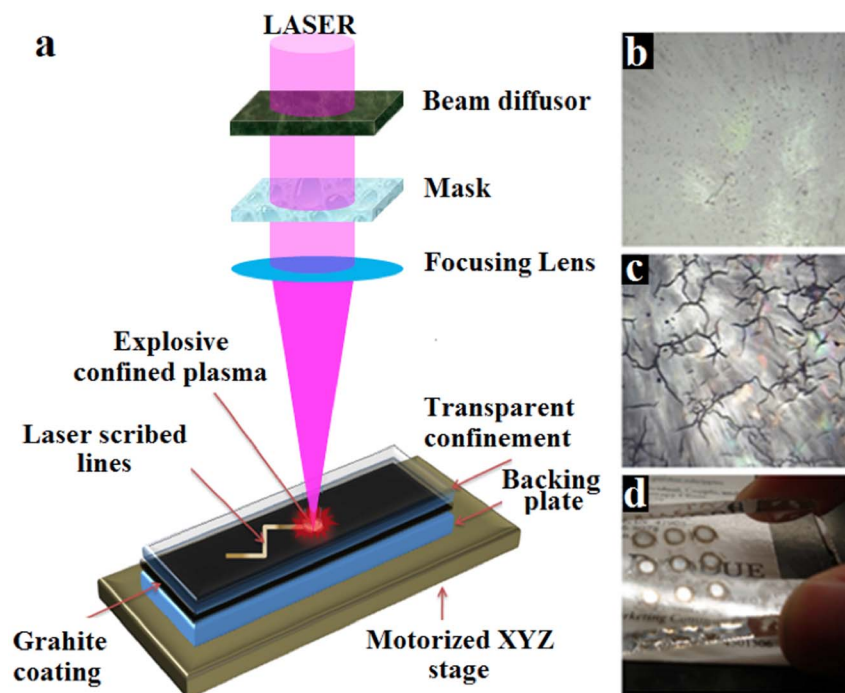


Figure 1 | the setup of confined pulse laser deposition (CPLD) and representative optical images of obtained carbon films. (a) Schematic diagram of the setup for CPLD. A pulsed laser beam is directed to pass through a beam diffuser to uniform its intensity distribution. A focusing lens is used to control the final spot size of laser beam. A homemade frame (not shown here) guaranteed close contact between the confinement, graphite coating and backing plate. When the laser beam transmits through the transparent layer and irradiates the coating layer, graphite vaporizes instantly and ionizes into hot plasma. The explosive plasma is bounced by the confinement and generates a localized high-temperature high-pressure environment. (b) and (c) are typical optical microscope pictures of amorphous carbon and nano-diamond films, respectively. Magnification: $10\times$. (d) Optical picture of spot array of semitransparent and conductive carbon films.

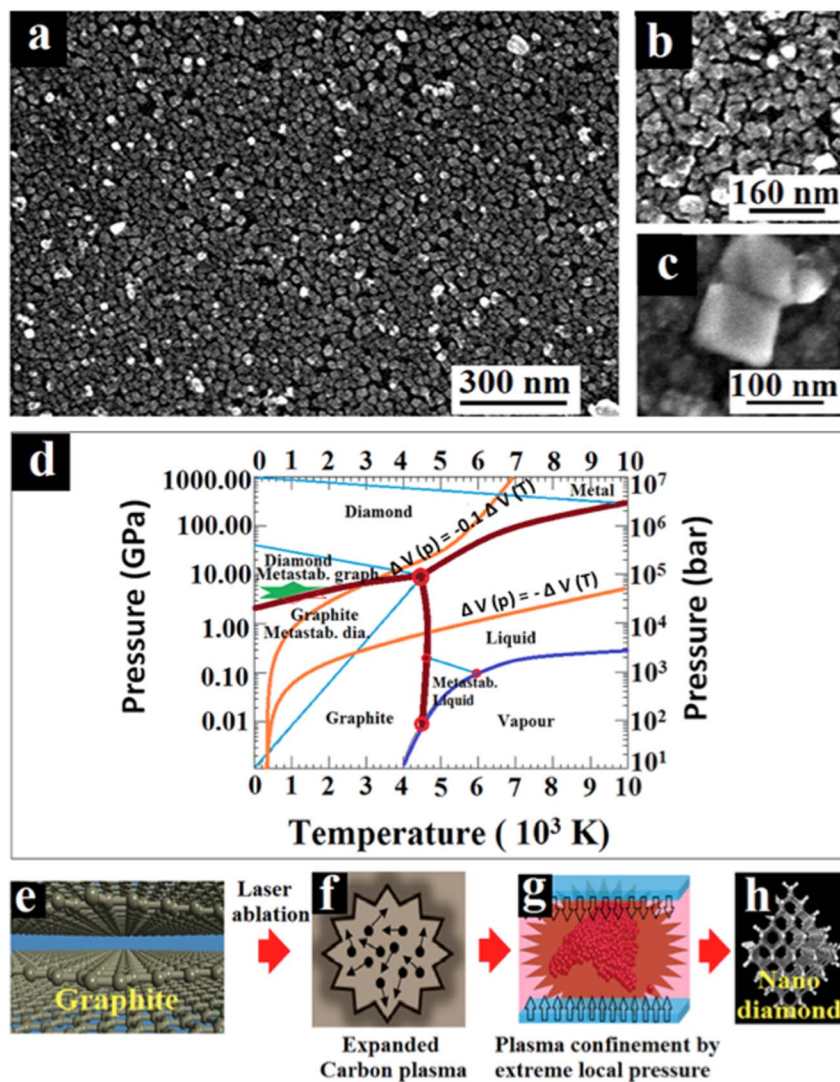


Figure 2 | Microstructures and synthesis process of nanodiamond. (a) and (b) are typical SEM pictures of dense nanodiamond film at different magnifications. Laser intensity: 5.8 GW/cm². (c) A cubic diamond nanocrystal with bigger size. These bigger nanocrystals scattered on the surface of carbon films. (d) Phase diagram of carbon. (green star represents the location in phase diagram corresponding to the present experiment). (e) – (h) Schematic diagram of synthesis process for diamond nanocrystals.

proposed that laser induced plasma source is one of the most promising approaches to diamond synthesis, because of its high activation efficiency and high deposition rate^{14,24}.

In this study, the laser processing of graphite under transparent solid confinement combines the advantage of both laser-induced high pressure and activated plasma by using low profile setup. As shown in the carbon phase diagram^{15,16} in Figure 2(d), metastable carbon plasma plume formation and graphite-diamond phase transformation can be activated when an instantaneous temperature rise is able to create a large pressure (2–100 GPa). Here, when a transparent solid confinement impede the laser ablated thermal expansion, a localized extreme condition is created close to iso-volumetric conditions. The impeded carbon expansion results in localized high pressure to enhance transforming graphite to nanodiamond. The localized high pressure induced by nanosecond laser can be calculated using Fabbro Model¹⁷. The shock wave impedance (Z) in the carbon-glass confinement interface was calculated by multiplying constant shock impedance of each of them together and the absorption fraction (α) is usually small (≈ 0.1 – 0.2). In this study, the interface shock wave impedance was calculated as 7.6×10^{-5} (g*s/cm²) and the absorption fraction was approximated as 0.1 to conservatively estimate the localized high pressure.

The physical process can be described in three stages^{17,24,25}, as illustrated in Figure 2e–f. In the first stage, the target is ablated by pulsed laser irradiation; graphite particles vaporize immediately and create a dense plasma plume. In the second step, the plasma explodes violently in the limited space and continues absorbing the laser energy as the laser pulse is applied (Figure 2e). The heating and condensation of the plasma result in the formation of a variety of carbon species including clusters, single atoms, and ions. Kinetic energies of these species are much higher than thermal energies. The third stage is the rapid quenching of the high-temperature high-pressure plasma (Figure 2f) and the formation of nanodiamond. It is obvious that laser-induced shock pressure and activated plasma in this process is advantageous for the formation of diamond phase carbon. As laser intensity increases, more number of energetic carbon species are activated²⁴, and higher local pressure is generated¹⁷. Thus more diamond phase carbon could form than graphite phase carbon from carbon vapor. In contrast to CPLD, it is very difficult for conventional pulse laser deposition to apply pressure needed for diamond transformation in the vacuum chamber²⁴.

We now have a bird's eye view on previous reports related to laser assisted nanodiamond formation. Narayan et al.¹¹ and Merkulov et al.¹² did not use any transparent confinement and therefore, their



methods required more extreme laser conditions for the nanodiamond formation. It should be noted that, they did not use various amorphous substrates such as glass and quartz which we used in the present study. Mistry *et al.*²³ went a step ahead to improve the process by employing multiple lasers to help rapidly coat a continuous nanodiamond film on various substrates. Due to lack of high pressure environment, which we have induced by confinement; Mistry *et al.* required extreme conditions for processing, which makes their process unrealistic and expensive. In this study, the transparent confinement glass is combined with single wavelength laser to induce both high pressure and activated plasma, which results in an effective nanodiamond formation and enables potential direct writing of the dielectric film on conducting graphite surface.

Figure 3 shows the variation of electrical resistance of the obtained films with different laser intensities. According to previous report^{26,27}, nanodiamond film contains sp^2 carbon along grain boundaries would have good conductivity. The resistance increases exponentially with the laser intensity and experiences a sudden change in power at about 3.7 GW/cm^2 , which indicates a carbon bond change from sp^2 to sp^3 and a phase transition of processed carbon films²⁸. The high resistance phase is attributed to diamond phase carbon, and low resistance phase is attributed to graphite phase carbon. According to the model of Fabbro *et al.*¹⁷, the local pressure can be evaluated under the confined configuration (Figure 3b). The calculation shows that laser intensity of 3.7 GW/cm^2 can induce a local pressure of about 4.4 GPa , which is close to the biaxial stress value (around 4.5 GPa) that can cause the onset of the transition from graphite like carbon to diamond like carbon during cathodic arc deposition²⁸. We note that carbon films deposited at low laser intensity show a good combination of high electrical conduction and optical transparency by adjusting deposition parameters (Supplementary Figure 1–3). Transparent conductors have a broad range of applications, such as in solar cells²⁹. Recently, great efforts have been

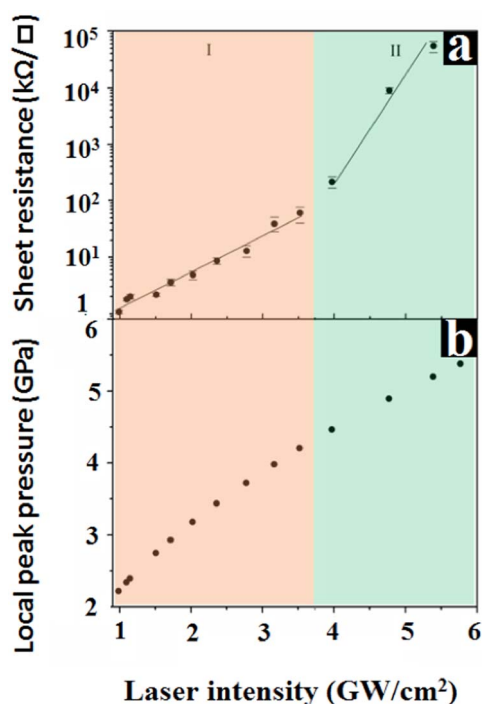


Figure 3 | (a) Sheet resistance of carbon films as a function of the laser intensity. The resistance is out of detection range when laser intensity is above 5.4 GW/cm^2 . The error bars show the standard deviations of electrical resistance for 10 measurements. The vertical dashed line indicates the critical laser intensity for phase transition. (b) Local peak pressure as a function of laser intensity.

devoted to finding a simple fabrication method for depositing transparent conductors in order to replace indium tin oxide (ITO). However, the use of amorphous carbon film as a transparent conductor is seldom mentioned.

This sp^2 to sp^3 bond change²⁸ also could be verified by X-ray photoelectron spectroscopy (XPS) observation^{30,31}. The XPS observation was operated in both wide survey (Figure 4(a)) and high-resolution analysis of the core level C1s spectra (Figure 4(b)) to investigate the surface functional components. As shown in Figure 4(a), the wide XPS survey spectra represents an evidence of oxygen peak around 532 eV besides C1s peak located at 284.4 eV ^{30,31}. The appearance of oxygen results from the CPLD process operated in ambient environment. However, additionally, oxygen signal also could attribute to oxygen-containing molecules like water or oxygen absorbed on the surface of the nanodiamond particles³¹. Comprehensive deconvolution of C1s photoelectron peak is exhibited in Figure 4(b). The deconvolution spectra reveals that the spectral line shape of C1s core level is composed of two components, with a higher binding shoulder (detected at 284.4 eV) and lower one (detected at 285.3 eV). Similar to the previous advancements, these two shoulders are assigned to sp^2 bond and sp^3 bond of Carbon 1 s, respectively³⁰. Therefore, the fitting and the quantification of the C1s peak was performed by these two main components, showing 22% carbon bond has been changed from sp^2 to sp^3 (Figure 4(b)).

Mere existence of C1s sp^3 bond could be contributed by either nanodiamond or amorphous carbon^{30,32}. Therefore, X-ray diffrac-

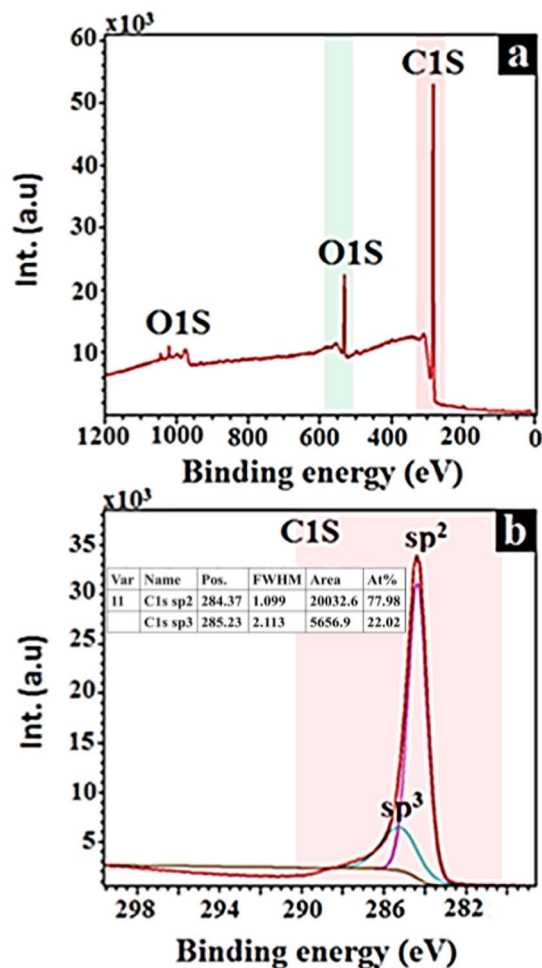


Figure 4 | (a) Wide XPS spectra of nanocrystalline diamond film direct laser deposited. (b) The deconvoluted spectra of high resolution C1s nanocrystalline diamond. Inserted text in (b) is the deconvolution output which indicating the ratio between C1s sp^2 bond and the sp^3 bond.



tion (XRD) was utilized to confirm the diamond phase^{33,34} in the sample processed by CPLD beyond the critical laser condition. Figure 5 shows the XRD pattern of the sample on Quartz substrate processed with laser intensity of 3.7 GW/cm². The diffraction pattern in Figure 5(a) exhibits a broad peak around $2\theta = 20.0^\circ$ is attributed to the quartz substrate. The sharp peak around $2\theta = 38^\circ$ is assigned to (111) peak of the aluminum sample holder, which is used for sample characterization³⁵. Nanodiamond (111) and Graphite (100) peaks stay close to each other in the XRD spectra, located at $2\theta = 44.0^\circ$ and $2\theta = 43.8^\circ$ with $\pm 0.05^\circ$ variation due to inherent strain in the sample, respectively^{36,37}. The sharp peak located around $2\theta = 43.8^\circ$ in Figure 5(a) is in good agreement with these two prior work^{36,37}. In order to distinguish the nanodiamond (111) peak and the Graphite (100) peak, the high resolution XRD was performed with center at $2\theta = 43.8^\circ$ to differentiate the diamond phase from graphite. The original 43.8 peak in Figure 5(a) is comprised of two components. At lower angle, higher intensity peak is attributed to Graphite (100) and a higher angle and lower intensity shoulder is attributed to the nanodiamond (111) peak. These two components can readily be decomposed by fitting to lorentzian lineshapes, as shown by the two green curves in Fig. 5(b). The fitting shows that the graphite peak is centered around 43.85° , which is consistent with previous work³⁷. Due to

the lack of crystallinity of the sputtered carbon/graphite, the FWHM of the graphite peak is quite large at 0.12° . This broadening spreads well into the area of the diamond peak. Fitting shows that the diamond peak is centered around 43.95° , with peak intensity 50% that of the graphite peak. The FWHM of nanodiamond peak is 0.13° , which corresponds to the grain size as observed in the TEM image (Figure 6). The diamond phase-graphite phase ratio can also be deduced from the peak fitting to be 11%, which is fitted by *Crystallmaker simulation* taking in account to parasitic like nanodiamond crystal size, defects, incident beam angle spreading and the sample roughness.

Furthermore, in order to investigate the nanodiamond crystals shown in Fig. 2, a high resolution transmitting electron microscope (HRTEM) observation was carried out. Figure 6 (a) presents the Low angle bright field images exhibiting the c-diamond crystal lattice. The average profile period of 2.07 \AA is corresponding to the $\langle 111 \rangle$ plane spacing of the diamond structure, which has been proved before^{36,38–40}. An area above the green box shows the Moire's pattern, which is due to the stacking of two different oriented grains. The grains with different orientation stack mainly due to the TEM sample preparation (sample was prepared by dispersing the nanodiamond into toluene, then dip coating onto TEM grid, finally soft baking to drive out the solvent).

Figure 6 (b) presents a chain of denotation nanodiamonds. The crystallinity and orientation of nanodiamonds with respect to one another are further studied by the angle analysis between the interface and the $\langle 111 \rangle$ lattice fringes and the selected area FFT patterns of different nanodiamond particles, respectively. Along the white line arrow in Figure 6 (b), with the $\langle 111 \rangle$ lattice planes clearly visible, we find the angle between the $\langle 111 \rangle$ planes to be 109° , which is consistent with the prediction that an interface between (111) facets will be stable³⁸. Nanocrystalline diamond with different orientations in Figure 6 (b) are marked with different colors, with nanodiamonds in size of tens of nms sitting together with interfaces. Figure 6c–k presents the FFT analysis of all the nanocrystalline diamonds marked in (b) corresponding to the color. While the yellow area exhibits low FFT signal and is difficult to analyze. The inserted ball-and-stick models are done with Crystal Maker simulation, showing the plane view of the nanocrystalline diamond orientation. Figure 6 (b) represents nanodiamonds with high crystallinity and different grain orientations, where the grain orientations are labeled by *Crystallmaker* with an incident beam along (001) shown in Figure 6c–k. The set of images clearly demonstrate the crystalline structure of the laser processed nanodiamond, and is in a good agreement with prior reports^{18,38,41,42}. Based on the FFT patterns, it can be concluded the nanodiamond particles have high crystal quality.

It is worth noticing that nanodiamonds become more stable than nano-scale graphite below 3–10 nm. When the size of diamond is reduced to about 3 nm, it is thermodynamically more favorable for it to have bare, reconstructed surfaces than hydrogenated surfaces. This inability to retain hydrogen at the surface prevents the growth of larger grains¹⁸. Due to the superior mechanical and thermal properties of nanodiamond, it provides an excellent filler material for nanocomposites. Due to the good biocompatibility and chemical stability, the nanodiamond are suitable for biomedical applications very well, e.g. drug delivery, in which nanodiamonds can provide a broad range of therapeutics, good dispersibility in water, good potential for targeted therapy and imaging¹⁹.

In conclusion, nanodiamond films and semi-transparent conductive carbon films were obtained by CPLD technique using nanosecond laser. Electrical measurement, XRD pattern and the TEM characterization revealed that there is a transition to graphite phase carbon and diamond phase carbon in the vicinity of 3.7 GW/cm². The critical value causes phase transition, since the photo energy reaches the required level to activate carbon vapor²⁵. It is worthwhile to study the potential to extend to other metastable materials pro-

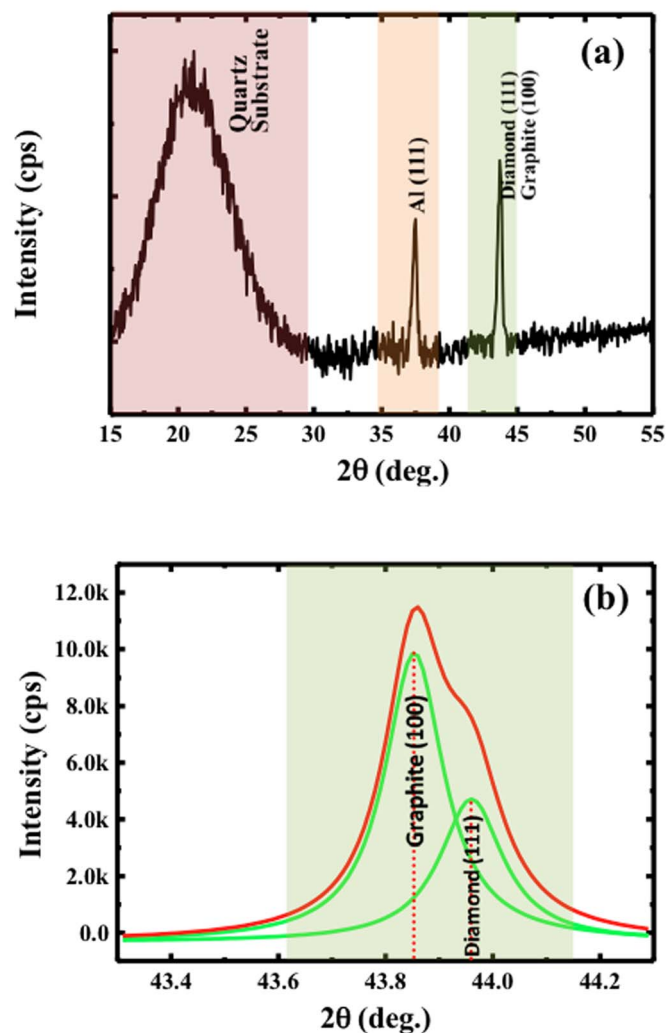


Figure 5 | (a) XRD patterns of the sample on Quartz substrate processed with laser intensity of 3.7 GW/cm². (b) The high resolution XRD was performed with center at $2\theta = 43.8^\circ$ to differentiate the diamond phase from graphite, and the green curves exhibit the deconvolution of the nanocrystalline diamond 111 peak.

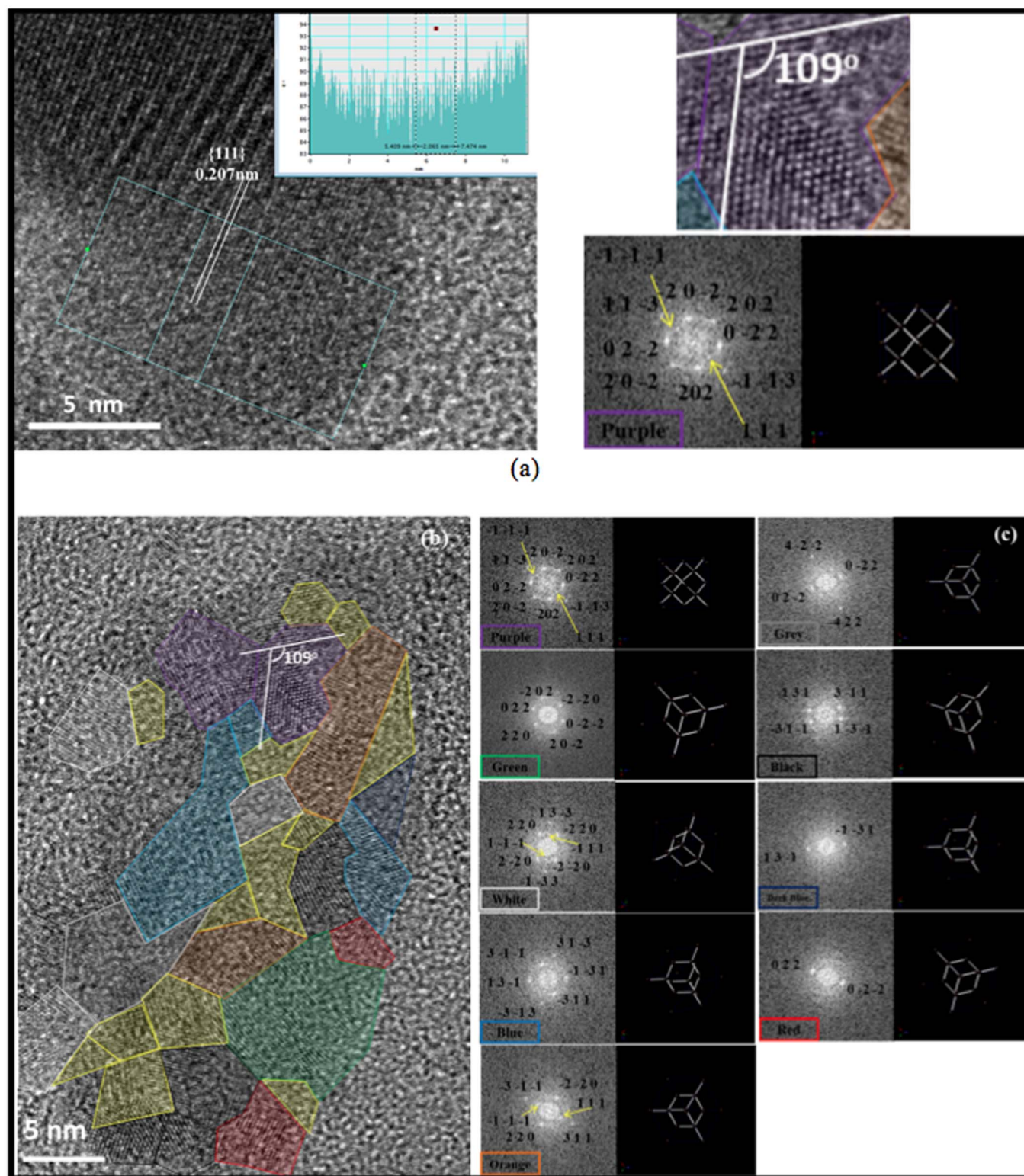


Figure 6 | (a) Bright field HRTEM images of the nanodiamond particles; the white lines indicate the orientation and separation of the lattice while inserted profile is the interlayer spacing of nanodiamond planes and FFT analysis of this diamond crystal. (b) HRTEM images of tens nm sized nanodiamonds sitting together with interface. Nanocrystalline diamond with different orientations is marked with different colors. (c) FFT analysis of all the nanocrystalline diamonds marked in (b) corresponding to the color, except yellow area which exhibits low FFT signal and is difficult to analyze. The inserted ball-and-stick models are done with Crystal Maker simulation, showing the plane view of the nanocrystalline diamond orientation.

duced by this method with different laser sources. Considering its super-fast speed, low cost, direct and flexible processing, CPLD has great potential to synthesize thin film of metastable materials.

Methods

A short pulse 248 nm KrF Excimer is used as the laser source. The pulse width of the laser is 25 ns, and the typical pulse energy is 300 mJ/pulse. The laser pulse energy is



measured using an optical power meter (Newport, type: 1916c). The beam diameter is calibrated by a photosensitive paper (Kodak Linagraph, type: 1895). The beam is shaped to 7×7 mm rectangle by beam shaper and then focused to micrometer by mirolens. Two batches of sample are prepared including graphite coating by spraying method and amorphous carbon thin film coated by SPI sputter™ coater. The graphite coating is obtained by spraying aerosol graphite lubricant (Asbury Carbons, USA) onto the backing plate. The aerosol graphite lubricant is a mixture of graphite particles and evaporable organic solvent. The thickness of graphite coating is in the range of $1 \sim 10$ μm . Glass or quartz plates are used as transparent confinement layers. The amorphous carbon thin film around 30 nm thick was coated by SPI sputter™ with carbon fiber target under 80 mtorr argon. The thickness was selected according to the laser penetration depth to obtain fully ablating the carbon film and creating the dense carbon vapor and plasma plume. The morphologies of the carbon films were characterized with a Hitachi S-4800 Field Emission SEM. The XPS spectrum was collected by the Kratos X-ray Photoelectron Spectrometer. The X-ray diffraction patterns were measured by the panalytical MRD X'Pert Pro High Resolution XRD. To characterize the HRTEM images with Titan 80–300 KV Environmental Electron Microscope, the sample was prepared by dispersing the produced nanodiamonds into toluene, then dip coating onto formvar TEM grid, finally soft baking to drive out the solvent. The sheet resistances were measured on a Jandel RM3-AR four point probing system.

CPLD is an ultra-fast process. The conversion efficiency depends on the laser intensity, repetition rate and wavelength. With higher laser intensity, the ionized carbon atoms accumulate higher kinetic energy and thus can be converted into higher percentage of nanodiamond. With shorter wavelength, e.g. deep UV laser, higher energy the photons will carry to interact with graphite, resulting in higher kinetic energy of carbon atoms. In terms of processing speed, if equipped with high power diode pump solid state (DPSS) laser with frequency of 50–100 kHz and a beam scanner, CPLD can generate nanodiamond thin films under ambient conditions with commercial scale.

- Hartl, A. *et al.* Protein-modified nanocrystalline diamond thin films for biosensor applications. *Nat Mater* **3**, 736–742, doi:10.1038/nmat1204 (2004).
- Praver, S. & Greentree, A. D. Applied physics. Diamond for quantum computing. *Science* **320**, 1601–1602, doi:10.1126/science.1158340 (2008).
- Nakagawa, K., Nishitani-Gamo, M. & Ando, T. Hydrogen production from methane for fuel cell using oxidized diamond-supported catalysts. *Int. J. Hydrogen Energy* **30**, 201–207, doi:DOI 10.1016/j.ijhydene.2004.03.038 (2005).
- American Institute of Physics. “Nano-diamond qubits and photonic crystals: Milestone reached on the path to integrated quantum technology.” ScienceDaily. ScienceDaily, 1 December 2010. <www.sciencedaily.com/releases/2010/11/101130100403.htm>.
- May, P. W. Materials science. The new diamond age? *Science* **319**, 1490–1491, doi:10.1126/science.1154949 (2008).
- Das, D. & Singh, R. N. A review of nucleation, growth and low temperature synthesis of diamond thin films. *Int. Mater. Rev.* **52**, 29–64, doi:DOI 10.1179/174328007x160245 (2007).
- Corentin, L. G., Fabrice, B., Tetsuo, I., Hiroaki, O. & Jean-Noël, R. Nanodiamond nucleation below 2273 K at 15 GPa from carbons with different structural organizations. *Carbon (New York, NY)* **45**, 636–648 (2007).
- Irifune, T., Kurio, A., Sakamoto, S., Inoue, T. & Sumiya, H. Materials: Ultrahard polycrystalline diamond from graphite. *Nature* **421**, 599–600, doi:10.1038/421599b (2003).
- Greiner, N. R., Phillips, D. S., Johnson, J. D. & Volk, F. Diamonds in Detonation Soot. *Nature* **333**, 440–442, doi:DOI 10.1038/333440a0 (1988).
- Angus, J. C., Will, H. A. & Stanko, W. S. Growth of Diamond Seed Crystals by Vapor Deposition. *J. Appl. Phys.* **39**, 2915–8, doi:DOI 10.1063/1.1656693 (1968).
- Narayan, J., Godbole, V. P. & White, C. W. Laser method for synthesis and processing of continuous diamond films on nondiamond substrates. *Science* **252**, 416–418, doi:10.1126/science.252.5004.416 (1991).
- Merkulov, V. I., Lowndes, D. H., Jellison, G. E., Puzetzyk, A. A. & Geohagan, D. B. Structure and optical properties of amorphous diamond films prepared by ArF laser ablation as a function of carbon ion kinetic energy. *Appl. Phys. Lett.* **73**, 2591–2593, doi:DOI 10.1063/1.122515 (1998).
- Mistry, P., Turchan, M. C., Granse, G. O. & Baurmann, T. New rapid diamond synthesis technique; using multiplexed pulsed lasers in laboratory ambients. *Mater. Res. Innovations* **1**, 149–156, doi:DOI 10.1007/s100190050033 (1997).
- Varnin, V. P., Laptev, V. A. & Ralchenko, V. G. The state of the art in the growth of diamond crystals and films. *Inorg. Mater.* **42**, S1–S18, doi:DOI 10.1134/S0020168506130012 (2006).
- Zazula, J. M. On Graphite Transformations at High Temperature and Pressure Induced by Absorption of the LHC Beam. *LHC Project Note* **78** (1997).
- Bundy, F. P. Pressure-Temperature Phase-Diagram of Elemental Carbon. *Physica A* **156**, 169–178, doi:DOI 10.1016/0378-4371(89)90115-5 (1989).
- Fabbro, R., Fournier, J., Ballard, P., Devaux, D. & Virmont, J. Physical Study of Laser-Produced Plasma in Confined Geometry. *J. Appl. Phys.* **68**, 775–784, doi:DOI 10.1063/1.346783 (1990).
- Mochalin, V. N., Shenderova, O., Ho, D. & Gogotsi, Y. The properties and applications of nanodiamonds. *Nat Nanotechnol* **7**, 11–23, doi:10.1038/nnano.2011.209 (2012).
- Galli, G. in *Computer-Based Modeling of Novel Carbon Systems and Their Properties* Vol. 3 *Carbon Materials: Chemistry and Physics* (eds Luciano Colombo & Annalisa Fasolino) Ch. 2, 37–56 (Springer Netherlands, 2010).
- Bundy, F. P. *et al.* The pressure-temperature phase and transformation diagram for carbon; Updated through 1994. *Carbon* **34**, 141–153, doi:DOI 10.1016/0008-6223(96)00170-4 (1996).
- Lifshitz, Y. *et al.* The mechanism of diamond nucleation from energetic species. *Science* **297**, 1531–1533, doi:10.1126/science.1074551 (2002).
- Palnichenko, A. V., Jonas, A. M., Charlier, J. C., Aronin, A. S. & Issi, J. P. Diamond formation by thermal activation of graphite. *Nature* **402**, 162–165 (1999).
- Pichot, V., Risse, B., Schnell, F., Mory, J. & Spitzer, D. Understanding ultrafine nanodiamond formation using nanostructured explosives. *Sci. Rep.* **3**, 2159, doi:10.1038/srep02159 (2013).
- Ong, H. C. & Chang, R. P. H. Effect of laser intensity on the properties of carbon plasmas and deposited films. *Physical Review B* **55**, 13213–13220, doi:DOI 10.1103/PhysRevB.55.13213 (1997).
- Voevodin, A. A. & Donley, M. S. Preparation of amorphous diamond-like carbon by pulsed laser deposition: A critical review. *Surf Coat Tech* **82**, 199–213, doi:DOI 10.1016/0257-8972(95)02734-3 (1996).
- Sankaran, K. J. *et al.* Gold ion implantation induced high conductivity and enhanced electron field emission properties in ultrananocrystalline diamond films. *Appl. Phys. Lett.* **102**, 061604, doi:DOI 10.1063/1.4792744 (2013).
- Liu, C. *et al.* Dielectric properties of hydrogen-incorporated chemical vapor deposited diamond thin films. *J. Appl. Phys.* **102**, 074115, doi:DOI 10.1063/1.2785874 (2007).
- Lau, D. W. *et al.* Abrupt stress induced transformation in amorphous carbon films with a highly conductive transition phase. *Phys. Rev. Lett.* **100**, 176101 (2008).
- Wang, X. *et al.* Transparent carbon films as electrodes in organic solar cells. *Angew. Chem. Int. Ed. Engl.* **47**, 2990–2992, doi:10.1002/anie.200704909 (2008).
- Mérel, P., Tabbal, M., Chaker, M., Moisa, S. & Margot, J. Direct evaluation of the sp³ content in diamond-like-carbon films by XPS. *Appl. Surf. Sci.* **136**, 105–110, doi:10.1016/S0169-4332(98)00319-5 (1998).
- Wang, X. F., Hasegawa, M., Tsugawa, K., Ruslinda, A. R. & Kawarada, H. Controllable oxidation of boron doped nanodiamond covered with different solution via UV/ozone treatment. *Diamond Relat. Mater.* **24**, 146–152, doi:DOI 10.1016/j.diamond.2011.12.033 (2012).
- Jackson, S. T. & Nuzzo, R. G. Determining Hybridization Differences for Amorphous-Carbon from the Xps C-1s Envelope. *Appl. Surf. Sci.* **90**, 195–203, doi:DOI 10.1016/0169-4332(95)00079-8 (1995).
- Liu, Y., Gu, Z. N., Margrave, J. L. & Khabashesku, V. N. Functionalization of nanoscale diamond powder: Fluoro-, alkyl-, amino-, and amino acid-nanodiamond derivatives. *Chem. Mater.* **16**, 3924–3930, doi:DOI 10.1021/Cm048875q (2004).
- Iakoubovskii, K. *et al.* Structure and defects of detonation synthesis nanodiamond. *Diamond Relat. Mater.* **9**, 861–865, doi:DOI 10.1016/S0925-9635(99)00354-4 (2000).
- Mukhopadhyay, D. K., Suryanarayana, C. & Froes, F. H. Structural evolution in mechanically alloyed Al-Fe powders. *Metallurgical and Materials Transactions A* **26**, 1939–1946, doi:10.1007/bf02670665 (1995).
- Qiao, Z. J., Li, J. J., Zhao, N. Q., Shi, C. S. & Nash, P. Graphitization and microstructure transformation of nanodiamond to onion-like carbon. *Scripta Mater.* **54**, 225–229, doi:DOI 10.1016/j.scriptamat.2005.09.037 (2006).
- Panich, A. M., Shames, A. I., Zousman, B. & Levinson, O. Magnetic resonance study of nanodiamonds prepared by laser-assisted technique. *Diamond Relat. Mater.* **23**, 150–153, doi:DOI 10.1016/j.diamond.2011.12.047 (2012).
- Chang, L. Y., Osawa, E. & Bernard, A. S. Confirmation of the electrostatic self-assembly of nanodiamonds. *Nanoscale* **3**, 958–962, doi:10.1039/c0nr00883d (2011).
- Welz, S., McNallan, M. J. & Gogotsi, Y. Carbon structures in silicon carbide derived carbon. *J. Mater. Process. Technol.* **179**, 11–22, doi:DOI 10.1016/j.jmatprotec.2006.03.103 (2006).
- Mutschke, H., Andersen, A. C., Jager, C., Henning, T. & Braatz, A. Optical data of meteoritic nano-diamonds from far-ultraviolet to far-infrared wavelengths. *Astronomy & Astrophysics* **423**, 983–993, doi:DOI 10.1051/0004-6361_20034544 (2004).
- Hamzah, E., Yong, T. M. & Yajid, M. A. M. Surface morphology and bond characterization of nanocrystalline diamonds grown on tungsten carbide via hot filament chemical vapor deposition. *J. Cryst. Growth* **372**, 109–115, doi:DOI 10.1016/j.jcrysgro.2013.02.009 (2013).
- Welz, S., Gogotsi, Y. & McNallan, M. J. Nucleation, growth, and graphitization of diamond nanocrystals during chlorination of carbides. *J. Appl. Phys.* **93**, 4207–4214, doi:DOI 10.1063/1.1558227 (2003).

Author contributions

Q.N. and Y.Y. did the experiments and wrote the manuscript. Y.W., J.S. and L.T. characterized the sample. J.L. and M.Y.Z. participated in experiments. G.J.C. designed the experiments and wrote the manuscript. All authors reviewed the manuscript.



Additional information

Supplementary information accompanies this paper at <http://www.nature.com/scientificreports>

Competing financial interests: The authors declare no competing financial interests.

How to cite this article: Nian, Q. *et al.* Direct Laser Writing of Nanodiamond Films from Graphite under Ambient Conditions. *Sci. Rep.* 4, 6612; DOI:10.1038/srep06612 (2014).



This work is licensed under a Creative Commons Attribution-NonCommercial-NoDerivs 4.0 International License. The images or other third party material in this article are included in the article's Creative Commons license, unless indicated otherwise in the credit line; if the material is not included under the Creative Commons license, users will need to obtain permission from the license holder in order to reproduce the material. To view a copy of this license, visit <http://creativecommons.org/licenses/by-nc-nd/4.0/>